This article has been accepted for publication in IEEE Transactions on Instrumentation and Measurement. This is the author's version which has not been fully edited and content may change prior to final publication. Citation information: DOI 10.1109/TIM.2025.3551443

FBG-FT-IMU: Multi-modal Measurement System for Acupuncture Manipulation

Qiaokang Liang, *IEEE Member,* Zhanjin Deng, Jianyong Long, *IEEE Member*, Xiao Wenxing, Jianqing Peng, *IEEE Member*, Xingfang Pan, Haiyan Ren, Yaonan Wang

***Abstract*—The quantification of acupuncture manipulation relies heavily on kinematic and dynamic parameters, crucial for the advancement of acupuncture intelligence. Therefore, this paper proposes a novel multi-modal measurement system tailored for acupuncture manipulation. This system integrates Fiber Bragg grating (FBG)-based Force/Torque sensors with an intelligent posture glove equipped with an inertial measurement unit (IMU), named FBG-FT-IMU. The Force/Torque measurement component utilizes three FBGs and achieves miniaturization(Diameter: 5mm), lightweight (0.7g), and high precision (Resolution: 0.019N/0.009N·mm) through clever elastic body design, mechanical modeling, finite element analysis, and 3D printing technology. Additionally, the accuracy of sensor creep and temperature compensation are 0.1% F.S. and 8% F.S., respectively. respectively. The intelligent posture glove, by analyzing the finger movement patterns of acupuncture manipulation, installs IMU sensors at corresponding joints to measure XYZ-axis angles, velocities, and accelerations during needling. The system can simultaneously collect 11 data points and has been tested on both simulated and real human skin, covering four conventional techniques. Furthermore, the system underwent classification testing of manipulation categories on multiple benchmark neural network models, demonstrating excellent accuracy. The highest Accuracy of FBG-FT-IMU reached 0.9519, significantly surpassing the cases of using FBG-FT (0.7513) or IMU (0.9314) individually. These results underscore the effectiveness and superiority of the data collection system, emphasizing its significance in comprehensively quantifying the acupuncture manipulation employed by acupuncture practitioners.**

***Index Terms*—Acupuncture manipulation, fiber Bragg grating, force/torque sensors, inertial measurement unit, multi-modal Measurement.**

I. INTRODUCTION

ACUPUNCTURE is a systematic therapeutic modality in traditional Chinese medicine [1], [2]. The needling technique in acupuncture to a certain extent determines its therapeutic efficacy. A proficient needling technique induces a sensation of soreness, numbness, and distention [3]. Different acupuncture manipulations exhibit significant variations, and the same needling technique shows marked differences between animals and humans; however, experienced practitioners using the same needling technique demonstrate similarity [4]. The modern development of the acupuncture discipline necessitates intelligence, and the quantification of the needling technique is one of the foremost challenges in the intellectualization of acupuncture [5]. Nevertheless, the medical field lacks abundant clinical data on acupuncture acupuncture manipulation [6]. Parameters for quantifying acupuncture manipulation are categorized into four types: operational parameters, kinematic parameters, dynamic parameters, and temporal parameters [7]. Among these, kinematic and dynamic parameters are the most significant as they can describe both the needling technique and the state of acupuncture.

Research in kinematics encompasses key parameters such as

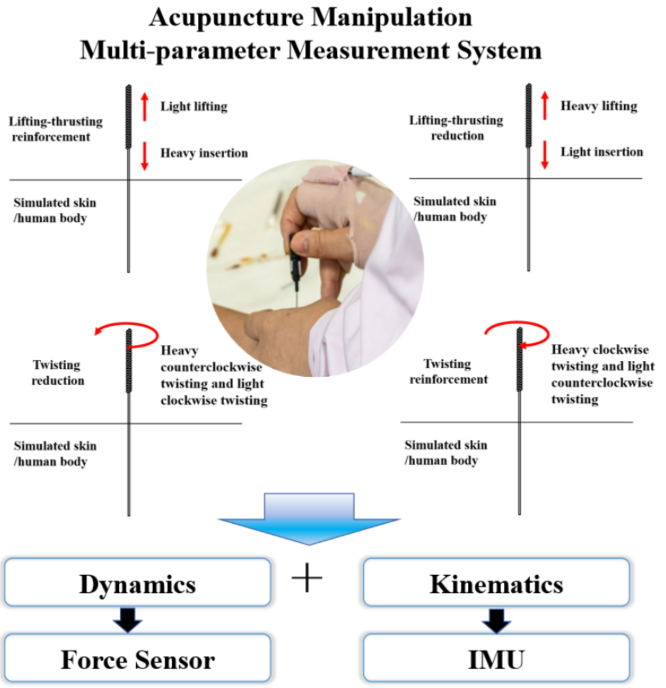

Fig. 1. The composition of the multi-modal measurement system for acupuncture manipulation and the structure diagram of the paper.

Manuscript received Month xx, 2024; revised Month xx, xxxx; accepted Month x, xxxx. This work was supported in part by the Project of the National Key Research and Development Program of China under Grant 2022YFB4703100, and in part by the National Natural Science Foundation of China under Grant 62303175 and 62073129. (Corresponding author: Jianyong Long).

Qiaokang Liang, Zhanjin Deng, Jianyong Long, Wenxing Xiao, and Yaonan Wang are with the National Engineering Research Center for Robot Vision Perception and Control, College of Electrical and Information Engineering, Hunan University, Changsha 410082, China (e-mail: qiaokang@hnu.edu.cn; dzj395@hnu.edu.cn; ljy_cv@hnu.edu.cn; Xiaowx126@hnu.edu.cn; yaonan@hnu.edu.cn).

Jianqing Peng is with the Sun Yat-sen University, Shenzhen 518107, China. (e-mail: pengjq7@mail.sysu.edu.cn).

Xingfang Pan and Haiyan Ren are with the Tianjin University of Traditional Chinese Medicine, Tianjin301617, China(e-mail:panxingfang@163.com, rhyxiaotong@163.com).

velocity, acceleration, amplitude, and angle [7]. One common method for accurately measuring these parameters is to install multi-axis motion sensors on the needle body [8]–[12]. However, the adhesive properties of sensors increase the weight and volume of the needle, affecting the tactile sensation of acupuncture practitioners. Therefore, some researchers opt to adjust the operating environment around the needle to obtain motion parameters without compromising operation. Yang et al. [13], [14] designed the "ATP-I Acupuncture Technique Parameter Determination Instrument," which employs variable resistance sensors to measure linear displacement, angular displacement, and frequency of the needle. Although kinematic parameters can effectively describe the motion of acupuncture manipulation, the introduction of dynamic parameters is particularly crucial in quantifying acupuncture manipulation due to the lack of the state of acupuncture [15].

The dynamical parameters of acupuncture typically included forces along different axes and their corresponding powers. Due to the presence of forces reliant on the interaction between objects, the measurement of dynamical parameters primarily relied on various types of mechanical sensors. In recent years, the research on the application of force sensors in medical robots has also been widely discussed by researchers [16]–[18]. Li et al. [19] developed a detection needle for acupuncture operations based on resistance strain gauge technology. The weight of this sensing needle was 10g, with a force measurement range of -1.5 to +1.5N and a torque measurement range of -5.5×10-4 to +5.5×10-4N·m. The measurement accuracies were 1.0×10-2N and 4.5×10-6N·m, respectively. Davis et al. [20] employed a novel acupuncture sensor tool named Acusensor to record real-time data of acupuncture. Research results demonstrated significant differences in displacement and rotation amplitudes between different needling styles, as well as significant differences in displacement frequencies among various acupuncture manipulations. Han et al. [21] investigated the relationship between axial torque and rotation angle or frequency, revealing a positive correlation between rotation angle and axial torque within a 180° rotation range, with a torque variation range of [0.023, 0.292]N·mm. Li et al. [22] mounted artificial skin on a six-axis force sensor with infrared, aiming to measure the kinematic and dynamic characteristics of acupuncture manipulation and concluding that consistency in action amplitude and velocity was a crucial feature for distinguishing between experts and novices. Son et al. [23] represented force sensor measurement data as friction coefficients using a modified Carnot friction model, quantifying the grasping sensation of acupuncture needles using the lifting and thrusting technique and conducting experimental verification with six tissue samples of varying hardness. Ding et al. [24] utilized resistance strain gauges as the measurement unit to design a force sensor for obtaining acupuncture manipulation, with a measurement range of torque: ±0.48N·mm and force: ±1.2N. This sensor enabled the objective recording of the needle during the needling process. Xu et al. [25] designed a miniaturized multi-axis force sensor using 3D printing, achieving axial force and torque measurement based on the strain gauge induction mode. The measurement range of this force sensor was torque: ±3N·mm, force: ±3N, with a sensor weight of 3g and a coupling error of less than 2%. Experimental results demonstrated the system's ability to accurately acquire needle force information and differentiate between different acupuncture manipulations. Compared to indirect measurement methods [26], the aforementioned direct measurement methods for force exhibited higher measurement accuracy, albeit with issues of large sensor weight and sensitivity that required further improvement [27]. It was difficult to measure the kinematic parameters of acupuncture directly and effectively using these methods.

In response to the aforementioned issues, this paper proposes a multi-modal measurement system for acupuncture manipulation consisting of two main components: the dynamics measurement component and a kinematic measurement component. The composition of the system and the structure of the paper are shown in Fig. 1. The dynamics measurement component primarily focuses on measuring Fz (force in the Z-direction) and Mz (torque around the Z-axis) using fiber Bragg grating (FBG) sensing technology. The force sensor's elastic body is ingeniously designed and fabricated using 3D printing technology, enabling high sensitivity, lightweight construction, and precise force and torque measurements. Furthermore, compared to capacitive, resistive, optoelectronic, and strain gauge-based force/torque sensors, FBG-based sensors offer advantages such as smaller size, higher sensitivity, immunity to electromagnetic interference, and excellent biocompatibility [28]–[31]. Furthermore, the multi-modal measurement system requires sensors to be non-electrical and easily sterilizable, both of which are inherent advantages of FBG-based sensors. On the other hand, the motion measurement component involves a glove equipped with attitude sensors to capture the kinematic parameters of the doctor during the acupuncture process. Finally, our system tests on simulated skin and the human body, and classifies four common acupuncture manipulations on the benchmark model. By integrating the force measurement component with the motion measurement component, comprehensive quantification of the techniques employed by the doctor during acupuncture can be achieved.

The remaining sections of this paper are organized as follows. Section II presents the composition of the multi-modal measurement system, as well as the measurement principles, modeling, and simulation of force/torque sensors. Section III discusses the static and dynamic experiments conducted on the sensors, performance comparisons with other sensors, and the testing and data validation of the multi-modal measurement system. Finally, Section IV concludes the paper and provides an outlook on future work.

II. PRINCIPLES AND DESIGN OF SYSTEM

A. Force Sensor Structure and Measurement System

The dynamic system (Force sensor) for acquiring acupuncture manipulation, as shown in Fig. 2(a), consists of three main components: the shell, elastic structure, and needle. It is primarily used to directly measure the interactive force and torque during the needling process in acupuncture. The shell, composed of a grip and sensor housing, contains a fiber optic channel within the grip. In the middle of the grip and sensor

This article has been accepted for publication in IEEE Transactions on Instrumentation and Measurement. This is the author's version which has not been fully edited and content may change prior to final publication. Citation information: DOI 10.1109/TIM.2025.3551443

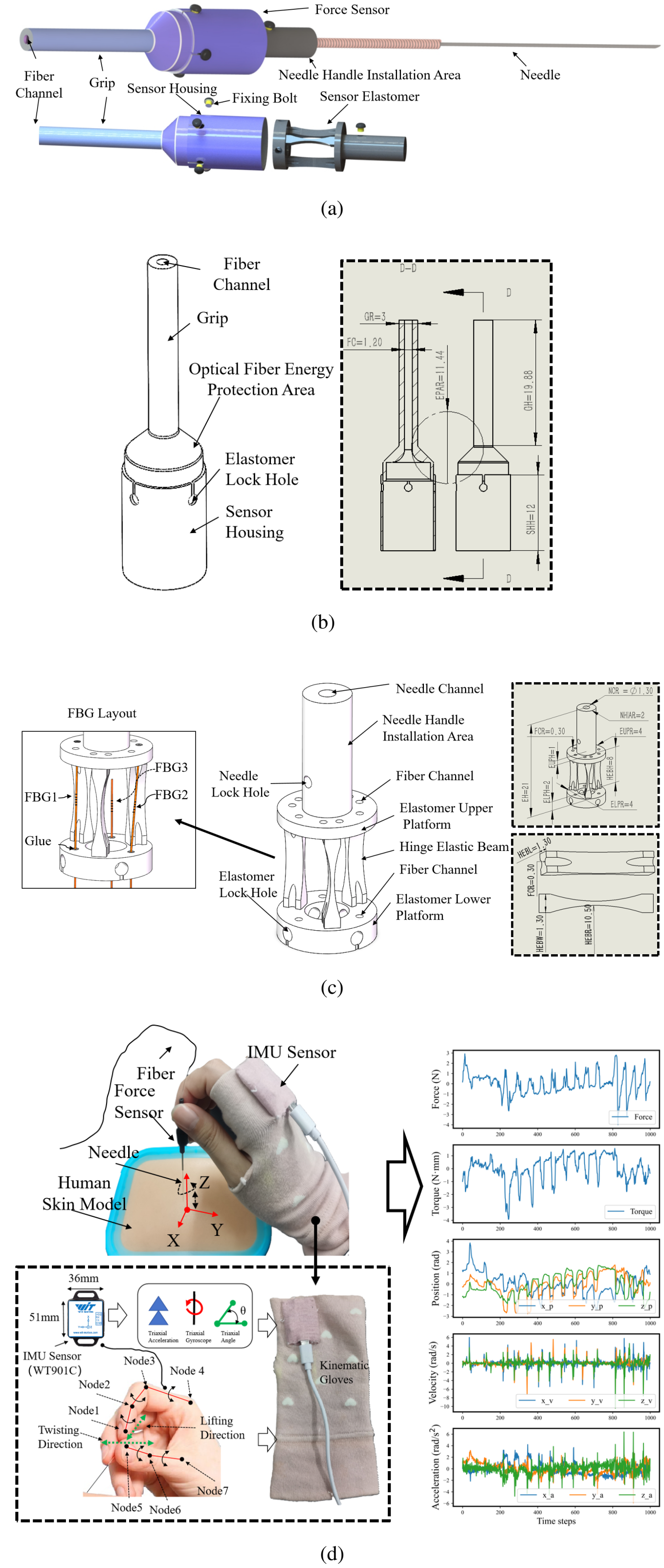

Fig. 2. (a) Assemble schematic of the designed sensor. (b) Schematic of shell. (c) Schematic of elastomer. (d) Schematic of the multi-modal measurement system and data collected.

housing, there is a fiber energy protection area that allows for a minimum bending radius of the fiber greater than 5mm, ensuring minimal energy loss and preventing fiber breakage. The external surface of the sensor housing has four elastomer lock holes evenly distributed at 90° intervals, which can secure the elastic structure of the sensor housing using fixing bolts. Refer to Fig. 2(b) for specific dimensions of the shell. The elastic structure of the dynamic system, as shown in Fig. 2(c), consists of three hinge elastic beams arranged vertically at 120° intervals. These hinge elastic beams enhance the sensor's sensitivity, particularly for torque measurements [27]. Both the upper and lower platforms of the elastic structure have fiber optic channels. The upper platform has three fiber optic channels evenly distributed at 120° intervals. Openings are present along the root of the hinge elastic beams on both sides, forming three pairs of fiber optic channels. In this paper, three Fiber Bragg Gratings (FBGs) are used for force and torque measurements. The grating length of FBG1 and FBG2 is 5mm, and they are fixed in a similar parallel distribution by double-point bonding on the elastic structure. This parallel configuration allows simultaneous measurement of force and torque while facilitating their decoupling.By optimizing the design, we achieve the measurement of force and torque using only two FBGs instead of the conventional four. FBG3 is only fixed at one end while the other remains free to compensate for temperature changes. The upper platform of the elastic structure has a needle handle installation area with a needle handle channel for installing acupuncture needles, which can be secured using a needle lock hole. The entire elastic structure is fixed through elastomer lock holes.

The multi-modal measurement system for quantifying acupuncture manipulation, as depicted in Fig. 2 comprises two main modules: a force sensor and an Inertial Measurement Unit (IMU) sensor. The force sensor, based on fiber optic grating measurement, is utilized for capturing the interactive forces involved in the process of acupuncture needling and twisting, enabling measurements of force and torque. The IMU sensor (WT901C, wit@wit-motion.com) is employed for perceiving the angles, velocities, and accelerations in the X, Y, and Z directions within the operational space, with dimensions measuring 51mm × 36mm. Analysis of acupuncture manipulation indicates that practitioners commonly employ the thumb and index finger to grip the needle handle during needling procedures. During insertion, these two fingers firmly grasp the handle, with movement centered around the wrist, while during twisting, the thumb primarily rotates around Node7, and the index finger is around Node3 and Node4 (refer to Fig. 2). To ensure the accuracy of IMU measurements, positioning the sensors at the needle tip or fingertip is most rational. However, constrained by volume considerations to avoid interference with medical procedures, we opted to place the sensors at the Node3-Node4 junction of the index finger and securely fasten them onto a glove, forming a kinematic glove. In summary, our measurement system integrates kinematic and dynamic parameters, facilitating real-time measurements and enabling a more comprehensive analysis and quantification of acupuncture manipulation.

This article has been accepted for publication in IEEE Transactions on Instrumentation and Measurement. This is the author's version which has not been fully edited and content may change prior to final publication. Citation information: DOI 10.1109/TIM.2025.3551443

B. Mechanical Analysis of Elastomer

The designed sensor in this study has a force range of ±4N and a torque range of ±4N·mm. As shown in Fig. 3(a), the elastic structure can be simplified into three parts, with the flexible hinge beam being the primary component responsible for elastic deformation. The beam is parameterized in the XOY plane, as shown in Fig. 3(b), and theoretical modeling is performed accordingly. Fig. 3(c) and (d) illustrate the deformation of the hinge beam under the influence of the Fz force and Mz torque, respectively.

When the sensor is loaded with axial force F_Z, the force acting on a single flexible hinge is $F = \frac{F_Z}{3}$, resulting in axial strain Δ_F,which can be expressed as

$$\Delta_F = \int_{-h}^{h} \frac{F}{E \cdot 2bL} dy \tag{1}$$

The flexible hinge is symmetric about the X-axis. $L = d - \sqrt{r^2 - y^2}$will be substituted into this equation, with the height y expressed as angle θ. Then Δ_F can be expressed as

$$\begin{aligned}\Delta_F &= \frac{F}{Eb} \int_0^h \frac{1}{d - \sqrt{r^2 - y^2}} dy \\ &= \frac{F_Z r}{3Eb} \int_0^{\arcsin \frac{h}{r}} \frac{\cos\theta}{d - r\sin\theta} d\theta\end{aligned} \tag{2}$$

when the sensor is loaded with the torque of Z axis, each flexure hinge will receive a radial force $F_{\text{x}} = \frac{M_Z}{3R}$, where R is the distance from the center of the upper surface of the hinge to the center of the upper platform. The flexure hinge will produce radial strain Δ_M. According to the castigliano's second theorem, the radial strain Δ_M can be expressed as

$$\Delta_M = \int_{-h}^{h} \frac{M(y)}{EI(y)} \cdot \frac{\partial M}{\partial F} dy \tag{3}$$

where $M(y)$ is the torque of the hinge loading, E is the young's modulus, $I(y)$ is the section moment of inertia. The flexure hinge has a rectangular cross section and section moment of inertia can be expressed as $I(y) = \frac{2bL^3}{3}$. $L = d - \sqrt{r^2 - y^2}$ will be substituted into this equation, and Δ_M can be expressed as

$$\Delta_M = 2\int_0^h \frac{F_x y^2}{\frac{2}{3}Eb\left(d - \sqrt{r^2 - y^2}\right)^3} dy \tag{4}$$

when $y = r\sin\theta$:

$$\Delta_M = \frac{M_Z r^3}{REb} \int_0^{\arcsin \frac{h}{r}} \frac{\sin^2\theta\cos\theta}{(d - r\cos\theta)^3} d\theta \tag{5}$$

Because FBG1 and FBG2 are in inclined suspension state, the strain of the flexure hinge cannot directly reflect the strain of the FBG. The relationship between the axial strain of the two FBGs and the axial strain Δ_F and radial strain Δ_M of the flexure hinge is as follows:

$$\begin{cases}\Delta_1 = \sqrt{4\text{h}^2 + (l - \Delta_M)^2} - \sqrt{4\text{h}^2 + l^2} \\ \Delta_2 = \sqrt{(2\text{h} - \Delta_F)^2 + l^2} - \sqrt{4\text{h}^2 + l^2}\end{cases} \tag{6}$$

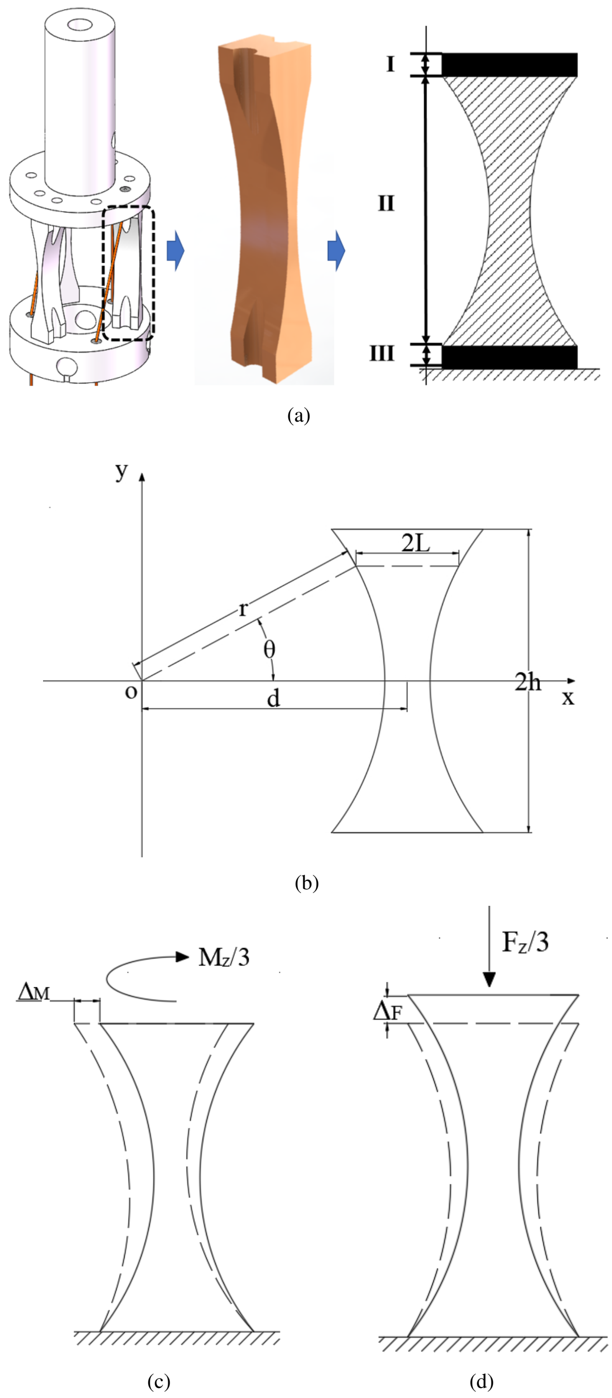

(a)
(b)
(c)
(d)

Fig. 3. (a) Schematic of one flexure hinge.(b)Schematic of coordinate xoy,(c)When loading F_Z, the deformation of one flexure hinge. (d)When loading M_Z, the deformation of one flexure hinge.

(6) Conversion available:

$$\begin{cases}\Delta_1 \approx -\frac{l}{\sqrt{4\text{h}^2 + l^2}}\Delta_M \\ \Delta_2 \approx -\frac{2h}{\sqrt{4\text{h}^2 + l^2}}\Delta_F\end{cases} \tag{7}$$

Based on the FBG sensing principle, the axial deformation of the optical fiber has a linear relationship with the temperature and central wavelength of the FBG. Therefore, the

This article has been accepted for publication in IEEE Transactions on Instrumentation and Measurement. This is the author's version which has not been fully edited and content may change prior to final publication. Citation information: DOI 10.1109/TIM.2025.3551443

space vector force and temperature can be simplified as a linear system, which can be expressed as

$$\begin{cases} \frac{\Delta\lambda_1}{\lambda_1} = (1-P_e)\frac{\Delta_1+\Delta_2}{\sqrt{4h^2+l^2}} + (\alpha_f+\zeta)\Delta T \\ \frac{\Delta\lambda_2}{\lambda_2} = (1-P_e)\frac{-\Delta_1+\Delta_2}{\sqrt{4h^2+l^2}} + (\alpha_f+\zeta)\Delta T \\ \frac{\Delta\lambda_3}{\lambda_3} = (\alpha_f+\zeta)\Delta T \end{cases} \tag{8}$$

Where $\sqrt{4h^2+l^2}$ is the initial suspension length of three FBG fibers, $\Delta\lambda_1$, $\Delta\lambda_2$ and $\Delta\lambda_3$ represent the axial strain of three FBGs. λ_1, λ_2 and λ_3 are the initial wavelengths of the optical fiber, which are 1541.96nm, 1538.02nm and 1544.98nm respectively, all around 1540nm. Therefore, the central wavelength of these fibers can be simplified as $\Delta\lambda_1 \approx \Delta\lambda_2 \approx \Delta\lambda_3 \approx \Delta\lambda_0$. The measurement matrix can be determined as follows:

$$\begin{bmatrix} \Delta\lambda_1+\Delta\lambda_2-2\Delta\lambda_3 \\ \Delta\lambda_1-\Delta\lambda_2 \\ \Delta\lambda_3 \end{bmatrix} = \left[C_1\right]_{3\times3} \begin{bmatrix} F_z \\ M_z \\ \Delta T \end{bmatrix} \tag{9}$$

where:

$$\left[C_1\right]_{3\times3} = 2\lambda_0 \begin{bmatrix} A1 & 0 & 0 \\ 0 & A2 & 0 \\ 0 & 0 & A3 \end{bmatrix} \tag{10}$$

$$A1 = \frac{2\left(1-P_e\right)hr\int_0^{\arcsin\frac{h}{r}} \frac{\cos\theta}{d-r\sin\theta}d\theta}{3\left(4h^2+l^2\right)Eb} \tag{11}$$

$$A2 = \frac{\left(1-P_e\right)lr^3\int_0^{\arcsin\frac{h}{r}} \frac{\sin^2\theta\cos\theta}{(d-r\cos\theta)^3}d\theta}{\left(4h^2+l^2\right)EbR} \tag{12}$$

$$A3 = \frac{\left(\alpha_f+\zeta\right)}{2} \tag{13}$$

C. Performance Study and Simulation Based on FEM

Finite element software Workbench was used in this study to simulate the strain of the elastic structure. When the elastic structure is subjected to the needle insertion force load, FBG1, and FBG2 exhibit strain output, while FBG3 remains unstrained as it is not fixed and therefore is not considered in the simulation. The elastic structure is made of black resin (https://formlabs.com/store/materials/black-resin/). Black Resin features a smooth matte surface and excellent mechanical properties, making it suitable for high-detail prototype production and sensor design. The material parameters for each component of the sensor are listed in TABLE I.

When subjected to an axial force (F_z) of 4N, the elastomer experiences strain, as depicted in Fig. 4(a). Both FBG fibers undergo simultaneous compression, resulting in identical strains in the same direction. At this 4N load, the maximum strain is $\varepsilon = 0.0018041$, corresponding to an equivalent stress of 4.691 MPa. Conversely, when loaded with a torque (M_z) of 4N·mm, the elastomer exhibits strain, as shown in Fig. 4(b). FBG1 and FBG2 exhibit strains of equal magnitude but in opposite directions. Under this 4N·mm load, the maximum strain is $\varepsilon = 0.020062$, with an equivalent stress of 52.161 MPa. Notably, the ultimate tensile strength of black resin is 65 MPa, indicating that the designed sensor can operate within its rated load. Modal analysis is conducted using Workbench to obtain the natural frequencies and vibration modes of the elastic body. Fig. 5 displays the relevant simulation results, showing the first five natural frequencies of the elastic body. As depicted in Fig. 5, the first mode of vibration corresponds to a uniaxial force directed towards the negative X-axis, with a natural frequency $f_1 = 1362.7Hz$. For the vibration modes associated with the other four natural frequencies, the second mode involves rotation about the X-axis, the third mode involves rotation about the Z-axis, the fourth mode entails a uniaxial force directed towards the negative Y-axis, and the fifth mode involves rotation about the Y-axis. The natural frequencies corresponding to these four modes are 1564.7, 2348.8, 5022.1, and 5175.6 Hz, respectively. Based on practical engineering experience, the maximum operational

TABLE I
MATERIAL PARAMETERS

Component	Material	Young's Modulus(GPa)	Poisson ratio	Density (Kg/m3)
Flexure	Black resin	2.6	0.4	1184
Optical fiber	Silica	72	0.17	2500
Glue	Epoxy resin	3.3	0.35	1180

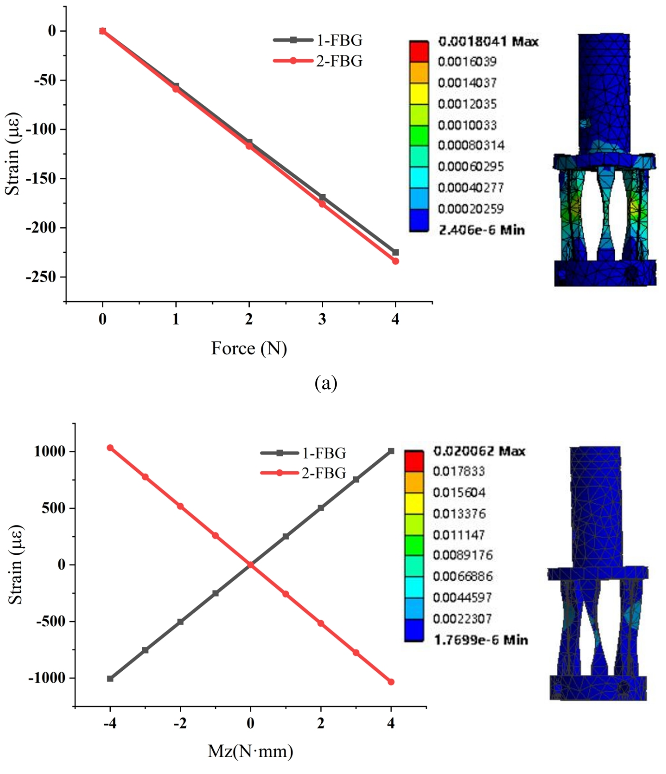

(a)

(b)

Fig. 4. (a)The simulation of elastomer and two FBG's strain when loading 4N. (b)The simulation of elastomer and two FBG's strain when loading 4N·mm

This article has been accepted for publication in IEEE Transactions on Instrumentation and Measurement. This is the author's version which has not been fully edited and content may change prior to final publication. Citation information: DOI 10.1109/TIM.2025.3551443

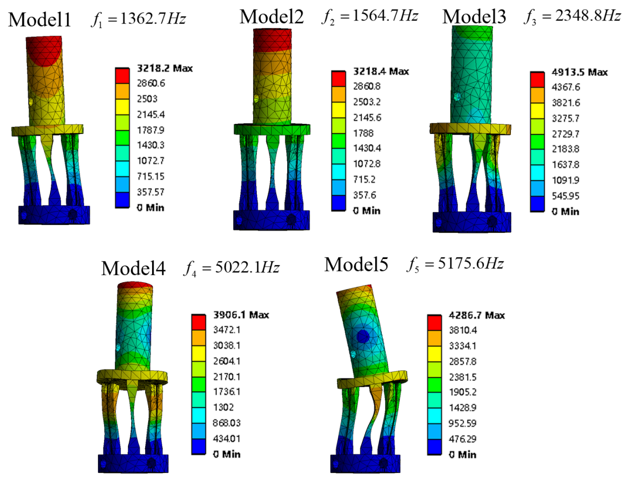

Fig. 5. First five natural frequencies and corresponding modal shapes of the elastomer.

frequency should be less than two-thirds of the first natural frequency. Therefore, the operational frequency range of the sensor is approximately 0-908 Hz.Our FBG-sensing system has a maximum sampling frequency of 100 Hz, which is adequate for acupuncture scenarios [32]. The bandwidth of the FBG sensor is contingent upon the optical fiber interrogator. Upgrading the interrogator's scanning frequency can enhance the bandwidth of the sensor system.

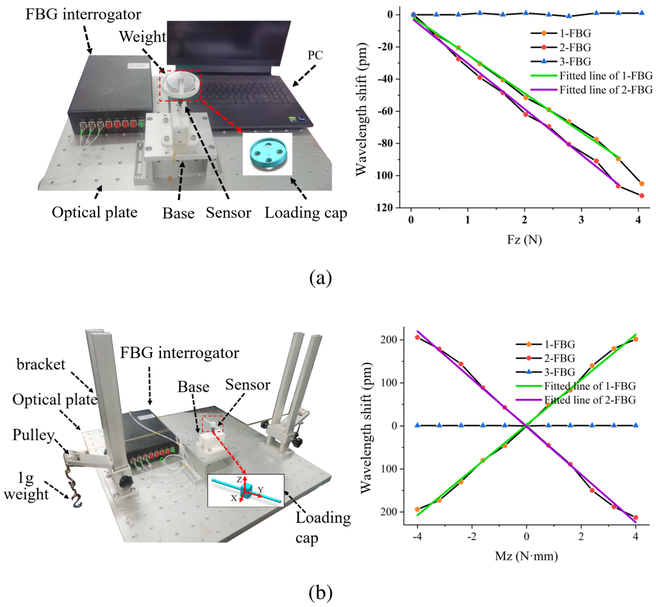

Fig. 6. (a)The equipment of force calibration platform and calibration result. (b)The equipment of torque calibration platform and calibration result.

III. EXPERIMENT AND ANALYSIS

A. Calibration Experiments

To establish the relationships of two dimensions between the strain and load on the sensor, two static calibration systems are constructed in this study, as shown in Fig. 6. The first system includes an optical plate, an FBG interrogator (the CASSTK-FT1611 with a frequency of 100 Hz and a resolution of 1 pm), a sensor base, a loading cap, and weights. Both the sensor base and the loading cap feature a central hole, designed for precise alignment and assembly with the grip and needle handle installation area of the designed sensor. This ensures that the designed sensor fits seamlessly into the sensor base and loading cap. The three FBGs of the designed sensor are connected to the interrogator. The weight of the calibration weights is recorded and wavelength signals are collected by a PC for further analysis. The second system comprises an optical plate, an FBG interrogator, an adjustable bracket, a pulley, a sensor base, a loading cap, and weights. The sensor base used in the first system and the second system is the same. The loading cap is designed to be installed on top of the designed sensor and can be loaded with a torque of 0.4N·mm using a 1g weight.

In the calibration experiments, the calibration ranges for the Z-axis axial force and torque on the sensor are (0, 4)N and (-4, 4)N·mm, respectively. Loading and unloading are performed with increments of 0.4N in the force dimension and 0.8N·mm in the torque dimension, repeated six times to construct the calibration dataset. The relationship between the center wavelength shift of FBGs and the external force and torque is determined using the average wavelength shift. The calibration results, depicted in Fig. 6 and TABLE II, demonstrate linear relationships between the wavelength shift of FBGs and the corresponding load. In the force dimension, FBG1 and FBG2 exhibit maximum sensitivities of 21.58pm/N and 29.80pm/N and hysteresis errors of 17.58% and 3.77%, respectively. The repeatability of the sensor is ±3.4%. Meanwhile, in the torque dimension, FBG1 and FBG2 demonstrate maximum sensitivities of 52.53pm/N·mm and 55.56pm/N·mm and hysteresis errors of 4.95% and 4.22%, respectively.The repeatability of the sensor is ±3.5%.

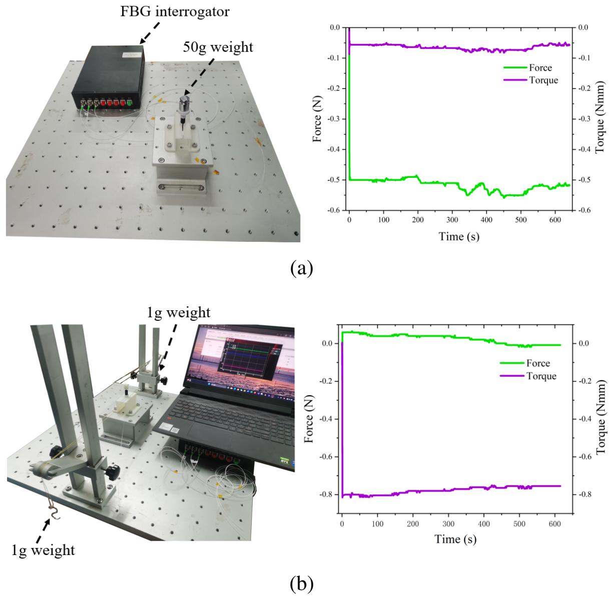

Fig. 7. (a)The equipment of force creep platform and creep result. (b)The equipment of torque creep platform and creep result.

This article has been accepted for publication in IEEE Transactions on Instrumentation and Measurement. This is the author's version which has not been fully edited and content may change prior to final publication. Citation information: DOI 10.1109/TIM.2025.3551443

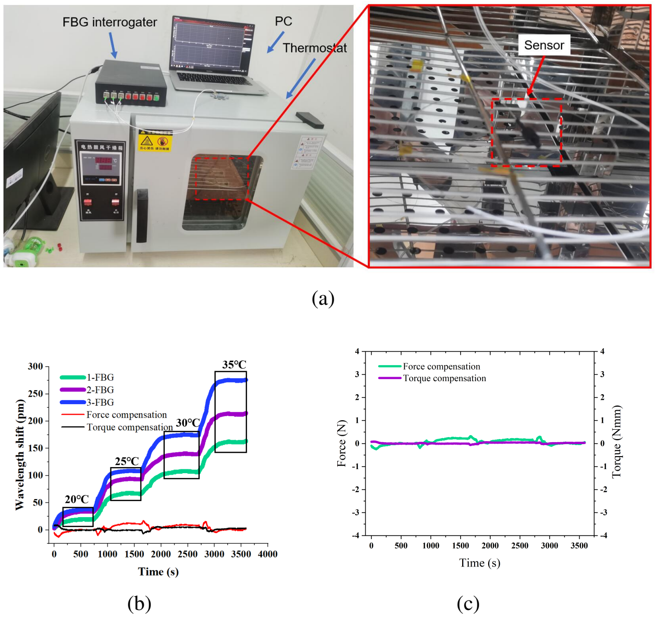

(a)

(b)

(c)

Fig. 8. (a) The equipment of temperature compensation experiment. (b) Three FBGs' wavelength shift and temperature compensation experiment results. (c) Temperature compensation for force and torque.

TABLE II
PERFORMANCE PARAMETER OF THE SENSOR

F/T	FBG	Sensitivity	Resolution	R-square
F_z	FBG1	21.58pm/N	0.046N/pm	0.99607
F_z	FBG2	29.80pm/N	0.034N/pm	0.9956
M_z	FBG1	52.53pm/N·mm	0.019N·mm/pm	0.9964
M_z	FBG2	55.56pm/N·mm	0.018N·mm/pm	0.99633

B. Creep and Temperature Compensation

The creep experimental platform is identical to the calibration platform. In the force creep experiment, the sensor is loaded with a 0.5N load and maintained for 10 minutes. In the torque creep experiment, the sensor is loaded with a 0.8N·mm torque and maintained for 10 minutes. It is important to note that in regular acupuncture procedures, the maximum values for force and torque are approximately 0.5N and 0.6N·mm, respectively, and the needle insertion process for each acupoint is typically completed within 1 min. Therefore, in this study, we conducted creep experiments within a reasonable and normal range by selecting a force of 0.5N, a torque of 0.8N·mm, and a duration of 10 min. The experimental results are shown in Fig. 7. When loaded with a 0.5N load, the maximum change in force is 0.05 N. When loaded with a 0.8N·mm torque, the maximum change in torque value is 0.05N·mm.

To assess the temperature compensation capability of the sensor, a temperature compensation experiment is conducted as depicted in Fig. 8(a). Given that the typical body temperature is approximately 37°C, the sensor is placed in a thermostat, and the thermostat temperature is set to 20°C, 25°C, 30°C, and 35°C for a duration of 10 minutes each. The FBG optical fibers are connected to the interrogator to record data, which is then stored in the computer for subsequent analysis. The experimental results, shown in Fig. 8(b), indicate a positive correlation between FBG wavelength shift and temperature, demonstrating good linearity. The temperature sensitivity coefficients of FBG1, FBG2, and 3-FBG are 9.44pm/°C, 12.06pm/°C, and 15.94pm/°C, respectively. Fig. 8(b) illustrates the raw FBG data after it has undergone temperature compensation. Fig. 8(c) shows the force/torque values output by the sensor following temperature compensation. In the temperature compensation experiment, the maximum variation in force is 0.32N, and the maximum variation in torque is 0.06N·mm.

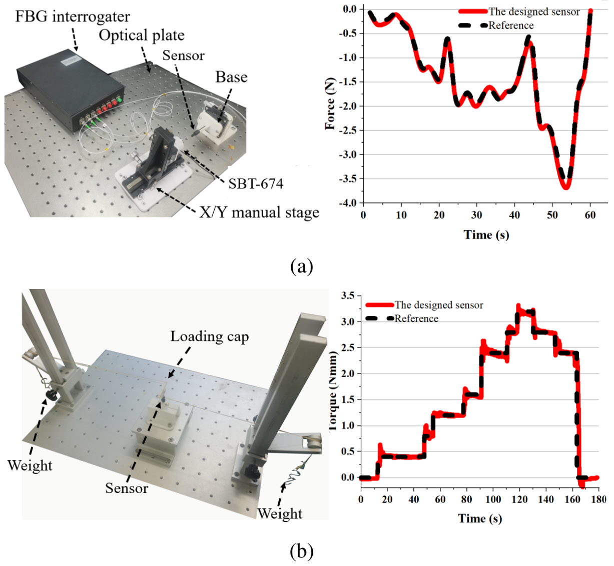

(a)

(b)

Fig. 9. (a) The equipment and comparison results of dynamic force experiments. (b) The equipment and comparison results of dynamic torque experiments.

During the temperature compensation experiment, the temperature coefficient ratios of the three FBGs are found to be different. To achieve temperature compensation, (9) should be converted:

$$\begin{bmatrix} \Delta\lambda_1+\Delta\lambda_2-1.35\Delta\lambda_3 \\ \Delta\lambda_1-\Delta\lambda_2+0.17\Delta\lambda_3 \\ \Delta\lambda_3 \end{bmatrix} = [C_1]_{3\times3} \begin{bmatrix} F_z \\ M_z \\ \Delta T \end{bmatrix} \tag{14}$$

Where:

$$[C_1]_{3\times3} = \begin{bmatrix} 51.38 & 0 & 0 \\ 0 & 108.09 & 0 \\ 0 & 0 & 15.94 \end{bmatrix} \tag{15}$$

C. Dynamic Performance Comparison

To assess the dynamic performance of the sensor, a dynamic experiment is conducted using the experimental platform as shown in Fig. 9. In the force dynamic experiment, we utilize a pressure sensor, the SBT-674, which has a range of 1 kg and an accuracy of 0.1%, along with an X/Y manual stage. The X/Y manual stage allows for the adjustment of the SBT-674 to align its axis with that of the sensor under test. The X/Y manual stage is manually controlled to perform random

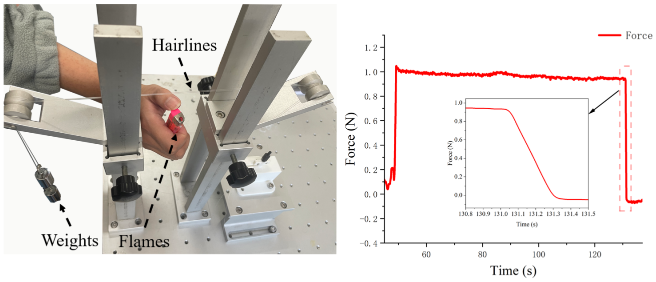

Fig. 10. The equipment of force perceptive experiment and result.

dynamic pressure tests with the SBT-674 and the sensor, with the results shown in Fig. 9(a). In the torque dynamic experiment, a platform similar to the calibration platform is selected to randomly apply or remove loads on the sensor. The results are depicted in Fig. 9(b). Data analysis indicates that the sensor exhibits excellent dynamic performance, ensuring a certain level of accuracy. In terms of force measurement, the maximum absolute error is 0.19N; for torque measurement, the maximum absolute error is 0.25N·mm.

To validate the dynamic sensitivity of the sensor, we design an experiment as illustrated in Fig. 10. A thin hairline passes through the hole in the Needle Handle Installation Area of the sensor, pulling the sensor vertically. The sensor is subjected to a constant load of 1 N. At 131 seconds into the experiment, the hairline is burned using a flame, causing the measured force to rapidly decrease from 0.94 N to -0.06 N within 0.28 seconds, stabilizing near the zero baseline. The sensitivity curve of the dynamic test is shown in Fig. 10.

D. Comparison of Acupuncture Manipulation Measurement Methods

The comparison of quantitative work of different acupuncture techniques is shown in TABLE III. In this comparison, Li [19] demonstrates the best comprehensive ability in resolution for both force and torque. However, its measurement range is limited, potentially resulting in force or torque values exceeding the measurement range. Han [21] has the smallest resolution for force but the largest for torque. Both sensors have a quality level of 10g, whereas an acupuncture needle weighs only 0.3g, leading to significant differences between the collected manipulation data and normal manipulation scenarios. Xu [25] effectively addresses these issues by substantially reducing mass while maintaining decent resolution. Our sensor has seen improvements in resolution compared to Xu, with the mass reaching 0.7g, and temperature compensation has been accomplished. Furthermore, the manipulation data acquisition system captures both dynamic and kinematic parameters, which are beneficial for manipulation classification, as outlined in Section III.E.

E. Effectiveness of the Measurement System

To assess the effectiveness of the measurement system, the acupuncture manipulation of three experienced Chinese acupuncturists was collected in this experiment. The data

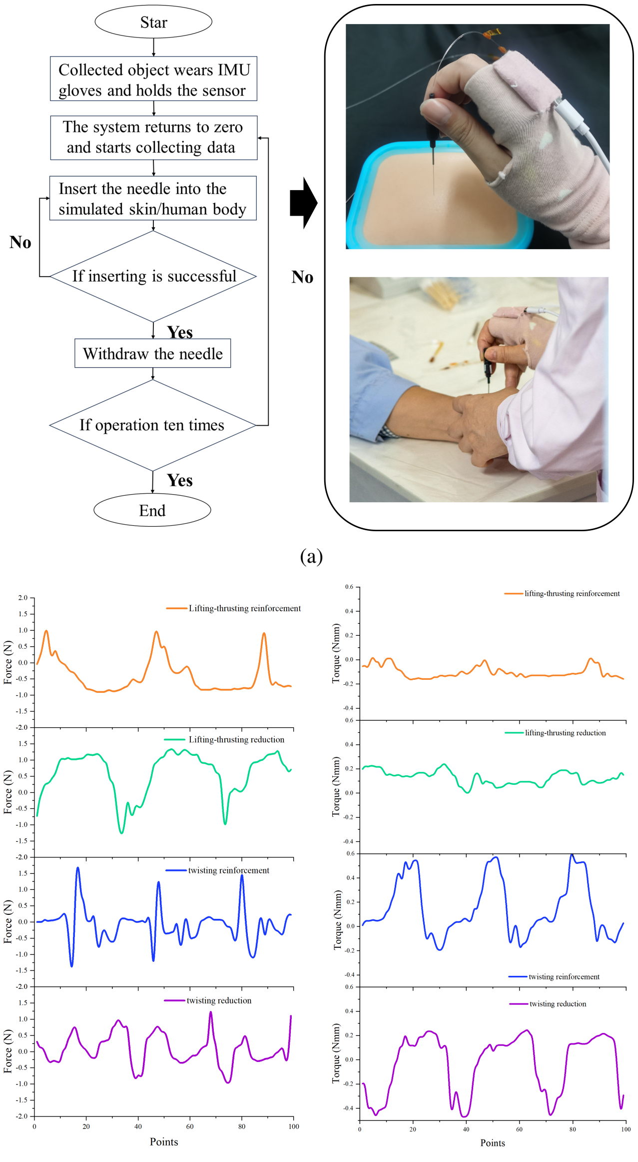

(a)

(b) (c)

Fig. 11. (a) A flowchart of multi-modal measurement system data collection process. (b) Force data of four acupuncture manipulations. (c) Torque data of four acupuncture manipulations.

TABLE III
COMPARISON OF ACUPUNCTURE MANIPULATION MEASUREMENT METHODS

Method	Range	Resolution	MP	TC	PT	SW(g)
Li [19]	±1.5N ±0.55N·mm	0.01N 0.005N·mm	SG	No	D	10
Han [21]	±35N ±250N·mm	0.006N 0.031N·mm	SG	No	D	10
Xu [25]	±3N ±3N·mm	0.026N 0.017N·mm	SG	No	D	3
Our sys	±4N ±4N·mm	0.019N 0.009N·mm	**FBG**	**Yes**	**D+K**	**0.7**

Note: MP=Measurement principle, TC=Temperature Compensation, SG =Strain Gauges, PT=Parameter Type, D=Dynamic, K=Kinematic

This article has been accepted for publication in IEEE Transactions on Instrumentation and Measurement. This is the author's version which has not been fully edited and content may change prior to final publication. Citation information: DOI 10.1109/TIM.2025.3551443

can be divided into four acupuncture manipulations including lifting-thrusting reinforcement, lifting-thrusting reduction, twisting reinforcement and twisting reduction [25]. Acupuncture manipulations are primarily categorized into lifting-thrusting and twisting. The terms reinforcement and reduction are used to describe the degree of entanglement between the needle tip and tissue fibers after the needle penetrates the skin. Greater entanglement corresponds to reinforcement, while less entanglement corresponds to reduction. As is shown in Fig. 11(a), the collected object wears gloves equipped with IMU in the system, and the gloves collect the posture data of node joints. Three experienced Chinese acupuncturists wear data collection equipment to perform four types of acupuncture manipulation on both simulated skin and human body acupuncture points. The specific collection process is shown in Fig. 11(a). The results of the data collected on force and torque during the acupuncture simulation on artificial skin are illustrated in Fig. 11 (b)-(c). It can be seen that there are obvious differences among the four acupuncture manipulations.

In theory, the force variations during the lifting-thrusting of acupuncture are more pronounced and periodic, while the torque variations during the twisting are more noticeable and also exhibit periodicity. Analyzing the data from Fig.11(b)-(c), it is evident that the amplitude of torque changes during lifting-thrusting is significantly smaller compared to the amplitude of torque changes during twisting. Moreover, the data indicate that the torque during lifting-thrusting still shows periodicity. This is because it is challenging for humans to perform a perfectly vertical lift and thrust, which results in the torque values also displaying periodic changes. Interestingly, the amplitude of force changes during twisting is similar to that of lifting-thrusting. During data collection, we observed that when doctors twist the needle, they often bend the needle handle, which introduces an elastic force on the needle, making the force changes during twisting similar to those during lifting-thrusting.

To further assess the effectiveness of the measurement system, we use the collected kinematic and dynamic parameters to recognize the acupuncture technique. We initially divided the long time-series data collected for each technique. Each sample consisted of 64 steps, with sampling occurring every 32 steps. Specifically, we collected 138, 89, 100, and 66 samples for each acupuncture manipulation, encompassing 11 data types, including 9 parameters from the IMU (Inertial Measurement Unit), as well as force and torque. After that, Z-score normalization is done for each sample divided. For any sample x, the Z-score normalization is done as follows:

$$x^{*} = \frac{x - \overline{x}}{\sigma} \tag{16}$$

where $\overline{x}$ and σ represent the mean and standard deviation of the raw data, respectively.

We divided the data into three categories: FBG-FT-IMU, FBG-FT, and IMU. These categories represent kinematic + dynamic data, dynamic data alone, and kinematic data alone, respectively. It is well-known that CNN models excel in handling spatial data, while LSTM models are adept at processing temporal data. Given that our acupuncture system combines kinematic parameters (IMU spatial data) and dynamic parameters (force/torque temporal data), adopting CNN-LSTM is more suitable. We employed a CNN-LSTM baseline model for training, and the training accuracy curve is shown in Fig. 12. The training results for performance metrics accuracy, precision, recall, and F1 score are summarized in TABLE IV. It is evident that the training results for FBG-FT-IMU data consistently outperformed the other two categories, highlighting the effectiveness and importance of our data collection system. Comparing the accuracy as the evaluation metric, the IMU data yielded a result of 0.9314, which was superior to the result obtained from FBG-FT data (0.7513). This indicates that kinematic data outperforms dynamic data in terms of technique classification, but falls short of the combined performance of both data types.

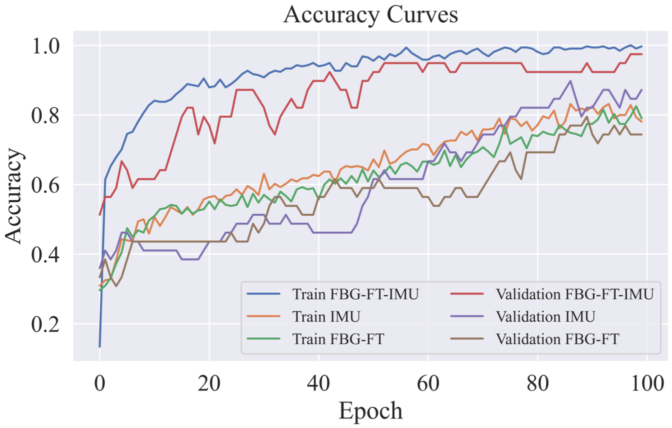

Fig. 12. The accuracy curve of three kinds of data FBG-FT, IMU, FBG-FT-IMU based on benchmark model CNN-LSTM respectively.

TABLE IV
DIFFERENT TYPES OF DATA ARE BASED ON THE CLASSIFICATION RESULTS OF THE BENCHMARK MODEL.

Model	Data type	Accuracy	Precision	Recall	F1 score
CNN-LSTM	FBG-FT	0.7513	0.7591	0.7209	0.7119
	IMU	0.9314	0.9334	0.9218	0.9199
	FBG-FT-IMU	**0.9519**	**0.954**	**0.9448**	**0.9453**

IV. CONCLUSION

In this paper, we proposed a method for quantifying acupuncture manipulations based on a multi-modal measurement system. This system integrates the measurement of mechanical and dynamic parameters and achieves comprehensive quantification of acupuncture manipulations by utilizing Fiber Bragg Grating (FBG) sensing technology and IMU data acquisition. Through systematic analysis of experiments including static calibration, creep, and temperature compensation, we validated the reliability and precision of the system. Dynamic performance comparison experiments indicated that our sensors possess excellent dynamic response capability, ensuring a certain level of accuracy. By collecting acupuncture operation data on simulated skin and human subjects, we demonstrated the potential of this system in capturing

This article has been accepted for publication in IEEE Transactions on Instrumentation and Measurement. This is the author's version which has not been fully edited and content may change prior to final publication. Citation information: DOI 10.1109/TIM.2025.3551443

acupuncture techniques and classified and identified different acupuncture techniques. In contrast, the classification results of using FBG-FT or IMU data alone were slightly inadequate, indicating that combining multiple parameter data can improve recognition accuracy and stability.This demonstrates the effectiveness of our Multi-modal Measurement System. Improving the success rate of manipulation classification or tackling more challenging tasks with a better algorithm is one of our future directions.

In summary, the multi-modal measurement system proposed in this paper provides a new method for the quantitative research of acupuncture manipulations, holding the potential for significant roles in clinical practice. Future work will continue to optimize system performance and further explore its application in evaluating acupuncture treatment effects and clinical practice.

REFERENCES

[1] Z. Yuan, Y. Peng, H. Yuan, L. Wang, S. Song, S. Chen, Y. Liu, H. Liu, H. Wang, G. Shi, C, Han, J. Cammon, Y, Zhang, J, Qiao, and G, Wang, “Effect of BCI-Controlled Pedaling Training System With Multiple Modalities of Feedback on Motor and Cognitive Function Rehabilitation of Early Subacute Stroke Patients,” *IEEE Transactions on Neural Systems and Rehabilitation Engineering*, vol. 29, no. 1, pp. 2569-2577, 2021.

[2] G. Tian, K. Qian, X. Li, M. Sun, H. Jiang, W. Qiu, X. Xie, Z. Zhao, L. Huang, S. Luo, T, Guo, R. Cai, Z, Wang, and B, Schuller, “Can a Holistic View Facilitate the Development of Intelligent Traditional Chinese Medicine? A Survey,” *IEEE Transactions on Computational Social Systems*, vol. 10, no. 2, pp. 700-713, 2023.

[3] S. Xin, C. Li, Y. Liu, H. Yuan, P. Zhang, J. Li, L. Ma, and J. Zhu, “A review of interventional factors influencing deqi of acupuncture,” *Journal of Clinical Acupuncture and Moxibustion*, vol. 28, no. 12, pp. 58-60, 2012.

[4] G. Ding, X. Shen. Y. Tao, H. Liu, W. Yao, and X. Li, “Comparative study on acupuncture techniques and needle body force parameters,” *Chinese Journal of Biomedical Engineering*, no. 04, pp. 334-341, 2004.

[5] H. Zhang, J. Liu, J. Song, and D. Wang, “Research progress of quantification and simulation application of acupuncture techniques,” *Shanghai Journal of Acupuncture and Moxibustion*, vol. 41, no. 05, pp. 528-534, 2022.

[6] H. Zhang, “Discussion of the present situation and development strategy of digital acupuncture and moxibustion,” in *Annual Meeting of China Association for Acupuncture and Moxibustion*, Jinan, China, 2022, pp. 597-601.

[7] R. Lyu, M. Gao, H. Yang, Z. Wen, and W. Tang, “Stimulation parameters of manual acupuncture and their measurement,” *Evidence-Based Complementary and Alternative Medicine*, Review vol. 2019, Aug 28 2019, Art no. 1725936.

[8] M. Q. H. Leow, T. Cao, S. L. Cui, and S. C. Tay, “Quantifying needle motion during acupuncture: implications for education and future research,” *Acupuncture in Medicine*, vol. 34, no. 6, pp. 482–484, 2016.

[9] Seo, Y. Lee, I. S. Jung, W. M. Ryu, H. S. Lim, J. Ryu, Y. H. Kang, J. W. and Chae Y, “Motion patterns in acupuncture needle manipulation,” *Acupuncture in Medicine*, vol. 32, no. 5, pp. 394–399, 2014.

[10] I.-S. Lee, Y.-S. Lee, H.-J. Park, H. Lee, and Y. Chae, “Evaluation of phantom-based education system for acupuncture manipulation,” *PloS One*, vol. 10, no. 2, Article ID e0117992, 2015.

[11] R. T. Davis, D. L. Churchill, G. J. Badger, J. Dunn, and H. M. Langevin, “A new method for quantifying the needling component of acupuncture treatments,” *Acupuncture in Medicine*, vol. 30, no. 2, pp. 113–119, 2012.

[12] X. Gu, “Development of teaching test apparatus for acupuncture manipulations in TCM,” *Chinese Acupuncture and Moxibustion*, vol. 21, no. 4, pp. 37-38, 2001.

[13] H. Yang, X. Gu, Z. Wang, and W. Yao, “Development and application of acupuncture manipulation parameter analyzer,” *Shanghai Journal of Acupuncture and Moxibustion*, vol. 22, no. 3, pp. 35-36, 1991.

[14] H. Yang, J. Xia, X. Gu, W. Wang, and B. Cheng, “Development of acupuncture manipulation parameter measuring instrument and analysis of manual force,” *Journal of Clinical Acupuncture and Moxibustion*, vol. 11, no. 6, pp. 51-52, 1995.

[15] H. M. Langevin, D. L. Churchill, J. R. Fox, G. J. Badger, B. S. Garra, and M. H. Krag, “Biomechanical response to acupuncture needling in humans,” *Journal of Applied Physiology*, vol. 91, no. 6, pp. 2471–2478, 2001.

[16] W. Lai, L. Cao, J. Liu, S. C. Tjin, and S. J. Phee, “A three-axial force sensor based on fiber bragg gratings for surgical robots,” *IEEE/ASME Transactions on Mechatronics*, vol. 27, no. 2, pp. 777–789, 2021.

[17] T. L. Li, F. Y. Chen, Z. B. Zhao, Q. F. Pei, Y. G. Tan, and Z. D. Zhou, “Hybrid data-driven optimization design of a layered six-dimensional fbg forcemoment sensor with gravity self-compensation for orthopedic surgery robot,” *IEEE Transactions on Industrial Electronics*, vol. 70, no. 8, pp. 8568– 8579, 2023.

[18] L. Xiong, Y. X. Guo, G. Z. Jiang, X. L. Zhou, L. Jiang, and H. H. Liu, “Six-dimensional force/torque sensor based on fiber bragg gratings with low coupling,” *IEEE Transactions on Industrial Electronics*, vol. 68, no. 5, pp. 4079–4089, 2021.

[19] Q. Li, F. Li, and B. Ai, “Research of detecting acupuncture needle for acupuncture manipulation,” *Chinese Journal of Sensors and Actuators*, vol. 19, no. 2, pp. 285–288, 2006.

[20] R. T. Davis, D. L. Churchill, G. J. Badger, J. Dunn, and H. M. Langevin, “A new method for quantifying the needling component of acupuncture treatments,” *Acupuncture in Medicine*, vol. 30, no. 2, pp. 113–119, 2012.

[21] Y.-J. Han, S.-Y. Yi, Y.-J. Lee, K.-H. Kim, E.-J. Kim, and S.-D. Lee, “Quantification of the parameters of twisting–rotating acupuncture manipulation using a needle force measurement system,” *Integrative Medicine Research*, vol. 4,no. 2, pp. 57–65, 2015.

[22] J. Li, L. E. Grierson, M. X. Wu, R. Breuer, and H. Carnahan, “Perceptual motor features of expert acupuncture lifting-thrusting skills,” *Acupuncture in Medicine*, vol. 31, no. 2, pp. 172–177, 2013.

[23] Y.-N. Son, J. Kim, H.-s. Lee, K.-M. Shin, Y.-J. Han, and S.-D. Lee, “Friction coefficient for the quantification of needle grasp in the lifting-thrusting method,” *International Journal of Precision Engineering and Manufacturing*, vol. 15, no. 7, pp. 1429–1434, 2014.

[24] G. Ding, X. Shen, J. Dai, H. Liu, W. Yao, and X. Li, “Research and development on the dynamic system for detecting the force of acupuncture needle during the acupuncture process in the clinical practice of traditional Chinese medicine,” *Journal of Biomedical Engineering*, vol. 20, no. 1, pp. 121–124, 2003.

[25] J. Xu, and A. Song, “A miniature multi-axis force/torque sensor for acupuncture,” *IEEE Sensors Journal*, vol. 23, no. 7, pp. 6660-6671, Apr 1 2023.

[26] J. Su, Y. Zhu, and M. Zhu, “Hand-eye-force coordination of acupuncture robot,” *IEEE Access*, vol. 7, pp. 82154-82161, 2019.

[27] D. W. Lai, Z. X. Tang, J. C. Zhao, S. X. Wang, and C. Y. Shi, “Design and Validation of a Miniature Fiber Bragg Grating-Enabled High-Sensitivity Torque Sensor,” *IEEE Sensors Journal*, vol. 21, no. 18, pp. 20027-20035, Sep 2021.

[28] J. Li, C. Wang, Z. Mao, Y. Liu, Z. Wang and H. Liu, “A Compact FBG-Based Triaxial Force Sensor With Parallel Helical Beams for Robotic-Assisted Surgery,” *IEEE Transactions on Instrumentation and Measurement*, vol. 71, pp. 1-9, Jun 2022.

[29] T. Li et al., “Multimode Proximal Force FBG-Based Sensors With High-Resolution for Catheter Surgical Robots,” *IEEE Transactions on Instrumentation and Measurement*, vol. 72, pp. 1-12, 2023.

[30] J. Long, Q. Liang, W. Sun, Y. Wang and D. Zhang, “Ultrathin Three-Axis FBG Wrist Force Sensor for Collaborative Robots,” *IEEE Transactions on Instrumentation and Measurement*, vol. 70, pp. 1-15, 2021.

[31] T. Li, C. Shi, and H. Ren, “Three-Dimensional Catheter Distal Force Sensing for Cardiac Ablation Based on Fiber Bragg Grating,” *IEEE/Asme Transactions on Mechatronics*, Article vol. 23, no. 5, pp. 2316-2327, Oct 2018.

[32] R. Zhang, Li. Lao, K. Ren, Brian M. Berman, “Mechanisms of Acupuncture–Electroacupuncture on Persistent Pain,” *Anesthesiology*, 120.2(2014):482-503.

[33] P. Maus, J. Kim, O. Nocentini, M. Z. Bashir, and F. Cavallo, “The Impact of Data Augmentation on Tactile-Based Object Classification Using Deep Learning Approach,” *IEEE Sensors Journal*, vol. 22, no. 14, pp. 14574-14583, Jul 2022.

Qiaokang Liang (Member, IEEE) received the Ph.D. degree in control science and engineering from the University of Science and Technology of China, Hefei, China, in 2011.

He is currently a Professor with the College of Electrical and Information Engineering, Hunan University, Changsha, China, where he is also the Vice Director of the National Engineering Research Center of Robot Vision Perception and Control. His research interests include robotic perceptions, advanced robot technology, and application of artificial intelligence technology in perceptions.

ZhanJin Deng received B.S degree in mechanical engineering and automation from Hunan University, Changsha, China, in 2022, where he is currently pursuing the M.S degree with the College of Electrical and Information Engineering, Hunan University, Changsha, China.

His research interests include optical fiber sensing technology for medical and industrial robots.

Jianyong Long (Member, IEEE) received the Ph.D. degree in control science and engineering from Hunan University, China, in 2022, and the M.S. degree from the College of Information and Computer Engineering, Northeast Forestry University, Harbin, China, in 2017.

He works as an Associate researcher at Hunan University, China, and his main research interests are in machine learning, robotics, and mechatronics.

Wenxing Xiao received B.S degree in automation from Huazhong Agricultural University, Wuhan, China, in 2022, where he is currently pursuing the M.S degree with the College of Electrical and Information Engineering, Hunan University, Changsha, China.

His research interests include machine vision and robotics systems.

Jianqing Peng (Member, IEEE) received the Ph.D. degree in Department of Mechatronics and Automation from Harbin Institute of Technology, Shenzhen, China, in 2018. He was a Postdoctoral Research Fellow of Harbin Institute of Technology in the Control Science and Engineering, from 2018 to 2020. He was also a research associate (Honorary) with the Department of Mechanical and Automation Engineering, The Chinese University of Hong Kong, Hong Kong, China, from 2019 to 2020.

He is currently an Associate Professor with the School of Intelligent Systems Engineering, Sun Yat-sen University, Shenzhen, China. His research interests include robotic control, robot vision, image processing, and redundant manipulator.

Xingfang Pan (Member, CAAM) received the Master of Medicine degree in School of Acupuncture-Moxibustion and Tuina from Tianjin University of Traditional Chinese Medicine, Tianjin , China, in 1999.

She is currently a professor with the School of Acupuncture-Moxibustion and Tuina, Tianjin University of Traditional Chinese Medicine, Tianjin, China. Her research interests include evaluation of clinical efficacy of acupuncture-moxibustion and evidence-based study of acupuncture-moxibustion.

Haiyan Ren M.D., graduated from the School of Traditional Chinese Medicine of Shandong University of Chinese Medicine in 2016 with a doctorate degree. She serves as the director of the Chinese Medicine Health Big Data Branch of China Information Society of Chinese Medicine, and the standing director of the Evaluation and Promotion Committee of TCM Suitable Technology of the World China Alliance Professional Committee.

At present, Ren Haiyan is the postgraduate supervisor of the School of Traditional Chinese Medicine of Tianjin University of Chinese Medicine, science and technology special commissioner, the third-level candidate of Tianjin ”131” innovative talent training project, and the young reserve talent of Tianjin colleges and universities. His main research interests are wisdom Chinese Medicine, standardization of Chinese medicine, etc.

Yaonan Wang received the B.S. degree in computer engineering from the East China University of Science and Technology (ECSTU), Fuzhou, China, in 1981, and the M.S. and Ph.D. degrees in electrical engineering from Hunan University, Changsha, China, in 1990 and 1994, respectively. He has been a Professor with Hunan University since 1995. His research interests include intelligent control and information processing, robot control, industrial process control, and image processing.

Dr. Wang is a fellow of the Chinese Academy of Engineering.